Nanoscale Res Lett (2009) 4:758–765
DOI 10.1007/s11671-009-9313-y

NANO EXPRESS

# Vegetable Oil-Based Hyperbranched Thermosetting Polyurethane/Clay Nanocomposites

**Harekrishna Deka · Niranjan Karak**

Received: 16 February 2009 / Accepted: 2 April 2009 / Published online: 25 April 2009


**Abstract** The highly branched polyurethanes and vegetable oil-based polymer nanocomposites have been showing fruitful advantages across a spectrum of potential field of applications. *Mesua ferrea* L. seed oil-based hyperbranched polyurethane (HBPU)/clay nanocomposites were prepared at different dose levels by in situ polymerization technique. The performances of epoxy-cured thermosetting nanocomposites are reported for the first time. The partially exfoliated structure of clay layers was confirmed by XRD and TEM. FTIR spectra indicate the presence of H bonding between nanoclay and the polymer matrix. The present investigation outlines the significant improvement of tensile strength, scratch hardness, thermostability, water vapor permeability, and adhesive strength without much influencing impact resistance, bending, and elongation at break of the nanocomposites compared to pristine HBPU thermoset. An increment of two times the tensile strength, 6 °C of melting point, and 111 °C of thermo-stability were achieved by the formation of nanocomposites. An excellent shape recovery of about 96–99% was observed for the nanocomposites. Thus, the formation of partially exfoliated clay/vegetable oil-based hyperbranched polyurethane nanocomposites significantly improved the performance.

**Keywords** Vegetable oil · *Mesua ferrea* L. seed oil · Nanocomposites · Hyperbranched polyurethane · Mechanical properties · Thermal properties

H. Deka · N. Karak (✉)
Advanced Polymer and Nanomaterial Laboratory,
Department of Chemical Sciences, Tezpur University,
Tezpur 784028, Assam, India
e-mail: karakniranjan@yahoo.com

## Introduction

Upgradation of the pristine polymers through the formation of nanocomposites is proven to be one of the best ways in recent time [1, 2]. Due to their high aspect ratio, stiffness, and in-plane strength, nanoclays are a choice of major polymer nanocomposite researches [3], as enhancement of properties like dimension stability, mechanical, thermal, flame retardancy, gas barrier, etc. are significant [4–8].

Again, two-phase morphology of the polyurethane, arising from the non-homogeneity of the hard and soft segments, makes it extraordinarily versatile [9, 10]. A wide range of physical and chemical properties can be tailor made just by judicious variation of composition and structure of three basic building blocks, viz., macroglycol, diisocyanate, and chain extender of polyurethanes or by physical modification like blending or through interpenetrating network formation with other polymers [11]. Thus, polyurethanes are being utilized in a diversified field of applications starting from coating and paint, foam, thermosetting, and thermoplastic elastomer to fiber [12]. However, some advanced applications demand high mechanical strength, chemical resistance, thermostability, low water vapor permeability, etc. Again, as the formation of exfoliated polyurethane/nanocomposites may eliminate the above short comings, in this study attempt has been made to investigate the same.

Again, hyperbranched polymers have been offering their candidature as an advanced polymeric material since the last two decades due to their highly functionalized three-dimensional globular non-entangled inimitable architectural features and unique properties [13]. These macromolecules exhibit many useful properties like improved solubility, low melt and solution viscosity, high reactivity, and so on for their different applications in

addition to their single-step preparative techniques [14–17]. Therefore, such novel macromolecules may be a right choice for this research.

Further, the present scenario of environmental issues, problems regarding disposal, reprocess, fast exhaustion of petroleum reserves, etc., have compelled us to use the renewable products including vegetable oils. These vegetable oils have the enormous advantages as they are biodegradable, renewable, sustainable, aptitude to facile modification, non-toxic, and the most importantly environmentally benign [18]. *Mesua ferrea* plant bears exceptionally high oil-containing (70%) seeds, and the favorable fatty acid composition of the oil enables its use for the preparation of polyurethane [19, 20]. Hence, the investigation of vegetable oil-based highly branched polyurethane nanocomposite is expected to offer high performance materials by coalescing the afore-stated advantages.

Authors herein wish to report the performance characteristics like mechanical, thermal, chemical, adhesive strength, water vapor permeability, etc. properties of *Mesua ferrea* L. seed oil-based HBPU/nanoclay nanocomposite at different dose levels of nanoclay. The shape memory behavior of the nanocomposites has also been investigated.

## Experimental

### Materials

*Mesua ferrea* L. seeds were collected from Darrang, Assam. The seed oil was isolated by solvent-soaking method and purified by the alkali-refining technique. Monoglyceride of the oil was prepared by the standard glycerolysis procedure. Glycerol (Merck, India) and poly(ε-caprolactone) diol (PCL, Solvay Co., $M_n = 3{,}000$ g/mol) were used after drying in an oven prior to use. Lead monoxide (S.D. Fine Chemical Ltd., Mumbai) and 2,4-toluene diisocyanate (TDI, Sigma Aldrich) were used as received. *N*,*N*-dimethylformamide (DMF, Merck, India) was vacuum distilled and kept in 4A type molecular sieves before use. Octadecylamine-modified montmorillonite clay (MMT) (Sigma Aldrich) of 25–30 wt% was used as nanoclay. Bisphenol-A-based epoxy resin (CY 250) and poly(amido amine) hardener (HY 840) (Ciba Geigy, Mumbai) were used as supplied. Other reagents are of reagent grade and are used without further purification.

### Preparation of HBPU and its Modification

The hyperbranched polyurethane was prepared by pre-polymerization technique. At first, the pre-polymer was prepared from 2 mol of poly(ε-caprolactone) diol, 3 mol of monoglyceride of *Mesua ferrea* L. seed oil, and 7.5 mol of TDI, and the polymer was obtained finally by the reaction of the pre-polymer with 2.5 mol of glycerol in DMF as a solution of 25–30% solid content (w/v). The molecular weight (Mw) of the polymer was $5.3 \times 10^4$ g/mol with polydispersity index 2.4, hydroxyl value 37.4 mg KOH/g, and the ratio of hydrodynamic radius with respect to linear analog 0.90.

In order to obtain thermosetting polymer composition, the above HBPU was mixed with 20 wt% (with respect to HBPU) of epoxy resin (100% solid content) and poly (amido amine) hardener (50% by weight with respect to the epoxy resin) at an ambient temperature by mechanical stirring followed by ultrasonication.

### Nanocomposites Preparation

Different amounts of the modified dispersed clay (1, 2.5, and 5 wt%) solution was added into the pre-polymer, which was obtained by the same procedure as described above. The nanoclay was dispersed in 1–5 mL of DMF by magnetic stirring followed by ultrasonication before adding into the pre-polymer. The remaining part of the preparation was the same as above. Finally, the nanocomposites films were obtained by solution casting, followed by vacuum degassing and curing at 120 °C for 45 min for further testing and analyses. The cured films were denoted as HBPU1, HBPU2.5, and HBPU5 corresponding to the clay content of 1, 2.5, and 5 wt%, respectively.

### Analysis and Characterization Techniques

FTIR spectra of the epoxy-cured hyperbranched polyurethane clay nanocomposites were recorded by a Nicolet (Madison, USA) FTIR Impact 410 spectroscopy using KBr pellets. The thermal analysis was done by a Simadzu, USA thermal analyzer, TG 50, at 10 °C $min^{-1}$ heating rate under the nitrogen flow rate of 30 mL $min^{-1}$. The DSC was done by Simadzu, USA, DSC 60, at 3 °C $min^{-1}$ heating rate under the nitrogen flow rate of 30 mL $min^{-1}$ from −50 to 80 °C. The measurement of specific gravity, impact resistance, hardness, flexibility (bending), and chemical resistance tests were performed according to the standard methods [19]. Gloss of the films was tested by mini gloss meter, Sheen Instrument Ltd., UK. The mechanical properties such as tensile strength and elongation at break were measured by universal testing machine (UTM) of model Zwick Z010, Germany with a 10-kN load cell and crosshead speed of 50 mm/min. The X-ray diffraction study was carried out at room temperature (ca. 25 °C) on a Rigaku X-ray diffractometer (Miniflex, UK) over the range of $2\theta = 1$–30° for the above study. Size and distribution of the nanoclay layers were studied by using JEOL, JEMCXII

transmission electron microscopy (TEM) at an operating voltage of 80 kV. Ultrasonicator (UP200S, Heishler, Germany) was used at various amplitude and continuous cycle for different time periods. The adhesive strength of the cured thin films was measured by lap shear test as per the standard ASTM D3165-95 procedure by using plywood sheets as the substrate. The water vapor barrier property was measured by taking 10 mL of water in the standard cup of 1 $cm^2$ cut on the lid. The nanocomposite films of 60–70 μm thickness were fixed in the lid, and the systems were kept in the vacuum oven under reduced pressure of 760 mm of Hg and at 25 °C. The initial weight of the cup with water and film is $W_0$. The percent weight loss through the films was calculated by measuring the weight of the cup ($W_1$) at specific intervals during the test using the following equation $(W_0 - W_1)/W_0 \times 100\%$.

The shape recovery test was done by heating the samples to 60 °C for 5 min followed by stretching to twice the length of the original length ($l_0$), and the stretched length is denoted as $l_1$. Immediately, the stretched samples were put in the ice water bath (2–3 °C) for 5 min to release the stretch, and the length was measured as $l_2$. The cooled samples were reheated to the same temperature (60 °C) for the same period of time, and the length obtained is denoted as $l_3$. The % of retention and % of recovery of the samples were calculated by the following equations:

$$\%\,\text{Retention} = (l_2 - l_0)/l_0 \times 100$$

$$\%\,\text{Recovery} = (l_1 - l_3)/l_0 \times 100$$

### Sample Preparation for Mechanical Properties

For impact resistance and scratch hardness studies, mild steel strips of 150 × 100 × 1.44 $mm^3$ were coated by the polymer nanocomposite solutions. Similarly, tin strips of 150 × 50 × 0.19 $mm^3$ were coated for bending and glass strips of 75 × 25 × 1.39 $mm^3$ were coated for gloss and chemical resistance test. All the films were found to be in the range of 60–70 μm thickness as measured by a Pentest coating-thickness gauge (Model 1117, Sheen Instrument Ltd., UK). The cured casted nanocomposites samples were cut by the manual sample cutter with dimension as per the ASTM D 412-51T for mechanical testing.

## Results and Discussion

### Preparation of HBPU and their Nanocomposites

Although the HBPUs have many advantages, the lack of mechanical strength is the main drawback which restricts its field of applications. The incorporation of the long segment in the main chain of a hyperbranched polymer can overcome this drawback [16]. In this study, HBPU is synthesized using the PCL macroglycol of molecular weight 3,000 g/mol as the long segment with monoglyceride of *Mesua ferrea* L. seed oil with excess TDI followed by the reaction of glycerol (Scheme 1). The macroglycol renders the high mechanical strength, whereas monoglyceride provides the benefit of vegetable oil. This HBPU was cured with epoxy resin and poly(amido amine) hardener to obtain thermosetting nanocomposites. Further, for better dispersion and delamination of the nanoclay layers, ultrasonication was employed along with mechanical agitation.

### Characterization

XRD is a powerful tool to investigate the degree of dispersion and delamination of clay layers in polymer matrix. In general, the intercalated layers show intense peak in the range of 1.5°–10° ($2\theta$ value), whereas exfoliated system gives no distinct peak in that range for their loss of structural integrity [21, 22]. Figure 1 shows the WAXD patterns for modified MMT, HBPU, and the nanocomposites. The d-spacing of the organically modified MMT was calculated on the basis of Bragg's equation and it shows diffraction peaks at $2\theta = 4.17°$, 19.97°, and 26.63° corresponding to d-spacings 2.36, 0.49, and 0.37 nm, respectively, for the pristine nanoclay. This peak was disappeared for the nanocomposites in XRD, which may be due to exfoliation (delamination) of nanoclay layers in the matrix by the polymer chains. Again, the modified HBPU exhibits two peaks at $2\theta = 21.2°$ (4.19 Å) and 23.4° (3.81 Å) which are due to (110) and (200) planes of PCL crystals in the structure [23]. The position of these two peaks remains unaltered after the formation of nanocomposites (Fig. 1). However, a closer visual probing reveals a trifle increase in the intensity of the two peaks. This increment in intensity resulting from enhancing the crystallinity is explained later on with the DSC result.

Further, the exfoliated structure of the clay layers in the nanometer range can be seen in the TEM images (Fig. 2). It provides a real picture what are happening inside the matrix. The clay layers approximately 10 nm thick are dispersed and disordered randomly in the matrix. This indicates that the clay layers are almost exfoliated and dispersed in the modified HBPU matrix.

The FTIR spectra of the epoxy-cured HBPU and nanocomposites are shown in Fig. 3. The distinctive absorption bands for the functional groups in the case of nanocomposites are almost similar to that of the HBPU (Fig. 3). The broadening of –NH stretching band was observed in the nanocomposites. This can be explained by the formation of the hydrogen bonding between the –NH of urethane with hydroxyl groups of the clay in addition to other possible groups present in the matrix. The change of band near

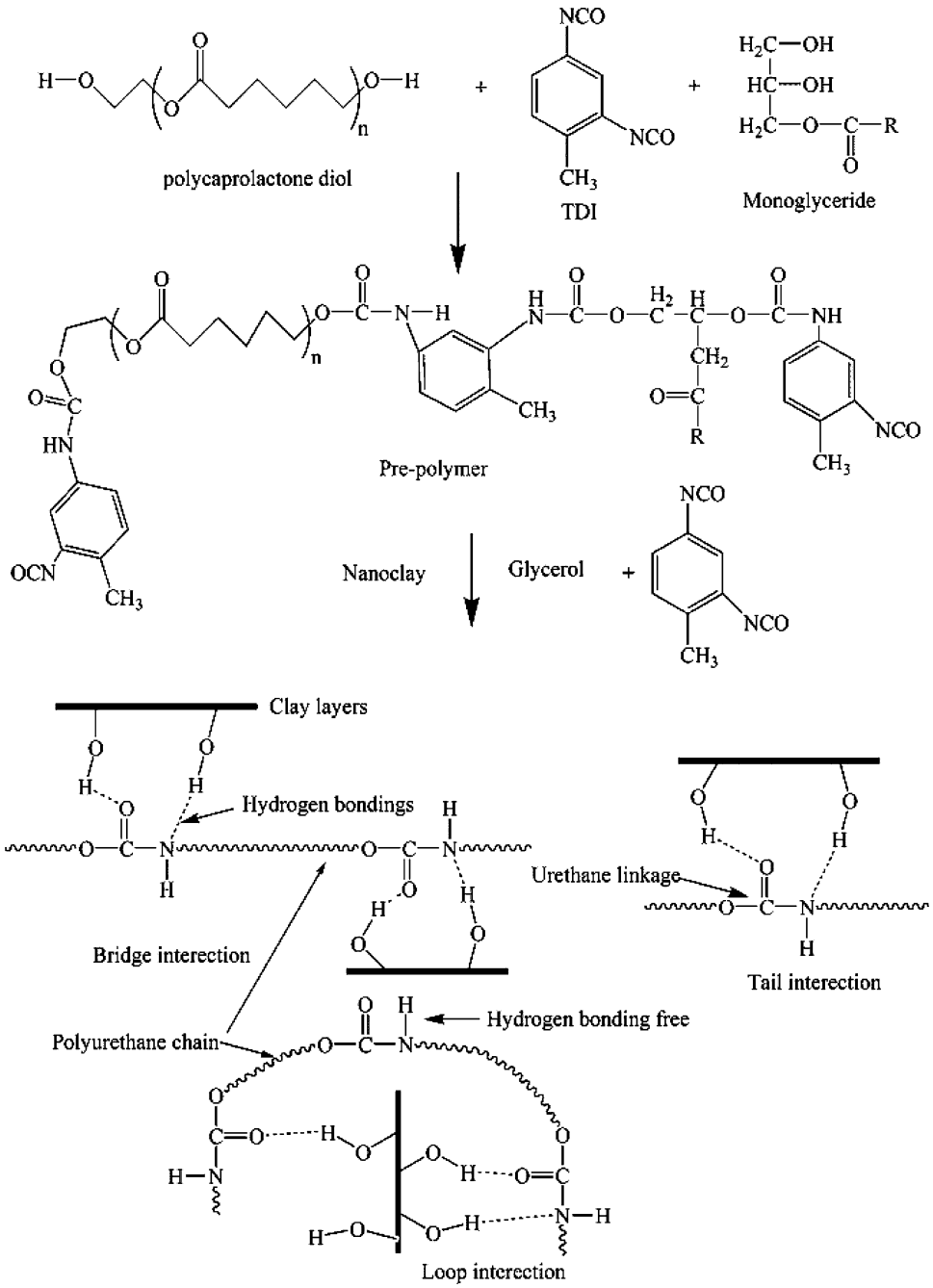


**Scheme 1** Proposed mechanism for interactions between nanoclay and matrix

1,600 $cm^{-1}$ may be due to the interaction of nanofiller with the HBPU through H bonding. The band appears in the pristine polymer, where the degree of hydrogen bonding is less, but while nanoclay is delaminated, the number of hydroxyl group is very high and thus strong H bonding between OH/NH and C=O was observed and the band enveloped. Although the dispersion state of the MMT layers cannot be observed directly from the IR data, their presence in the nanocomposites are inferred from the appearance of the absorption bands at 522 and 1,033 $cm^{-1}$ corresponding to Al–O and Si–O–Si stretching vibrations [11]. Further, the identical IR spectra taken from random parts of the nanocomposites tempt us to say that the organically modified MMTs are uniformly dispersed in the matrix. An attempt has been made to evaluate the microphase structure of the nanocomposites by FTIR. The urethane carbonyl region is the most helpful area to determine the hydrogen bonding [22]. The –C=O stretching vibration of urethane group is observed from 1,740 to 1,710 $cm^{-1}$ for the nanocomposites. The hydrogen-bonded –C=O group shows an absorption band at 1,710 $cm^{-1}$, while the free one shows at 1,740 $cm^{-1}$. The peak intensity ratio of

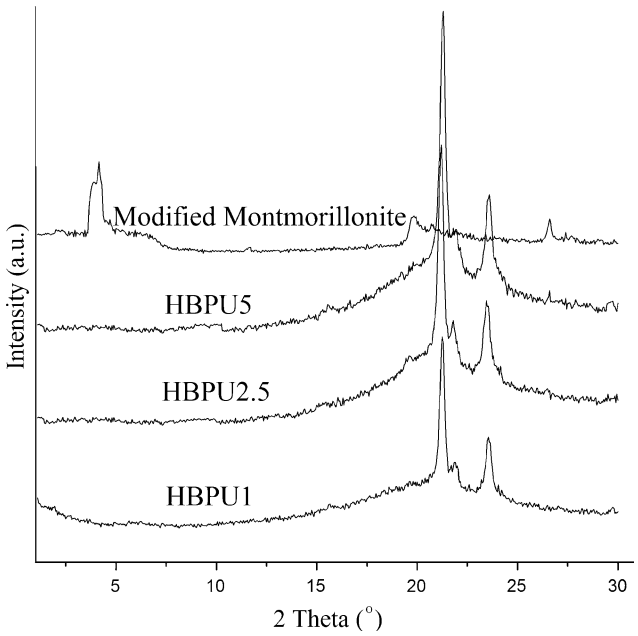


**Fig. 1** WAXD of the nanocomposites and modified montmorillonite

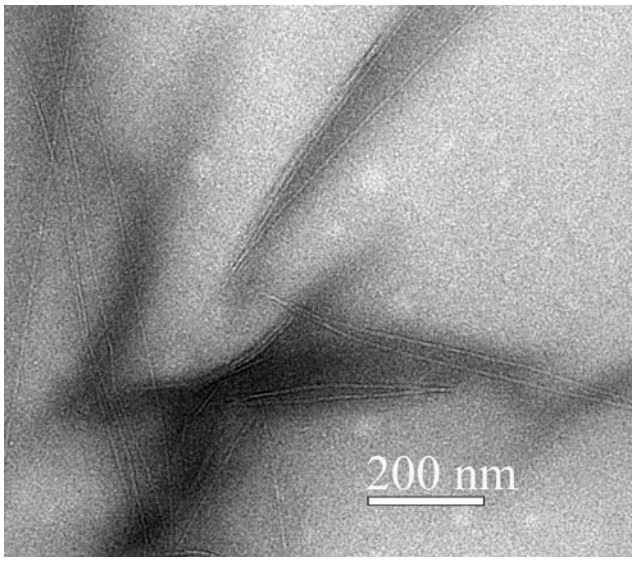


**Fig. 2** TEM micrograph of HBPU2.5 nanocomposite (representative one)

these two bands gives an estimate of the degree of hydrogen bonding. Thus, the hydrogen bonding index, $R$, may be defined as the ratio of absorptions $A_{1710}/A_{1740}$ [6]. The degree of phase separation (DPS) in the nanocomposites can be calculated from the peak intensity of the two bands following the equation:

$$\text{DPS}\,(\%) = C_{\text{bonded}}/(C_{\text{bonded}} + C_{\text{free}}) \times 100,$$

where C is the concentration of the bonded and free carbonyl groups.

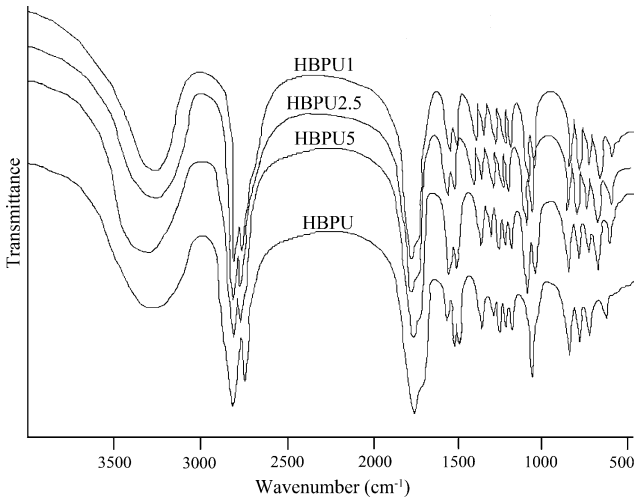


**Fig. 3** FTIR spectra of the HBPU and nanocomposites

It was observed that with the increase in clay content (1–5 wt%), the degree of phase separation increases (DPS values 47.2, 48.5 and 49.7 for HBPU1, HBPU2.5, and HBPU5, respectively). This may be due to the reaction of the –OH groups of the clay with the –NCO groups of the pre-polymer/TDI. Also, the greater strength of the hydrogen bonding between the –OH of clay and carbonyl group of urethane than intra-hydrogen bonding is attributed to the fact [22].

## Physical Properties

The retention of light-weight characteristic of the prepared nanocomposites is revealed from the density measurement. The densities of all the nanocomposites approximately remained the same compared with the pristine HBPU (Table 1). This is due to the addition of very little amount of clay (1–5 wt%), which may not influence the mass of the nanocomposites with respect to HBPU. The gloss of the nanocomposites was comparable with the similar type polymers prepared from the same vegetable oil [19, 20]. A decrease in the gloss of nanocomposites was observed from HBPU1 to HBPU5, which may be due the low gloss of the nanoclay. The transparent characteristic of the nanocomposites remains intact as seen from the Fig. 4. The retention of transparency of a transparent polymer is one of the properties of clay nanocomposite [3].

## Mechanical Properties

The mechanical properties of the nanocomposites are given in the Table 1. It was observed that the tensile strength of the nanocomposites increases with the increase of the nanoclay content, while the value for elongation at break decreases. This is because of the reinforcement of the

**Table 1** Physical and mechanical properties of nanocomposites and pristine polymer

| Properties | HBPU | HBPU1 | HBPU2.5 | HBPU5 |
|---|---|---|---|---|
| Impact resistance (cm) | 92 | 97 | 97.5 | 99 |
| Bending (dia. mm) | <5 | <5 | <5 | <5 |
| Gloss (60°) | 79.0 | 78 | 77 | 77 |
| Scratch hardness (kg) | 4.2 | 8.5 | 9.2 | 9.8 |
| Specific gravity | 1.16 | 1.17 | 1.19 | 2.00 |
| Tensile strength (MPa) | 30.20 | 40.03 | 45.62 | 48.1 |
| Elongation at break (%) | 510 | 472.17 | 454.36 | 440.21 |
| Lap-shear adhesion (MPa) | 6.42 | 8.56 | 9.31 | 11.68 |

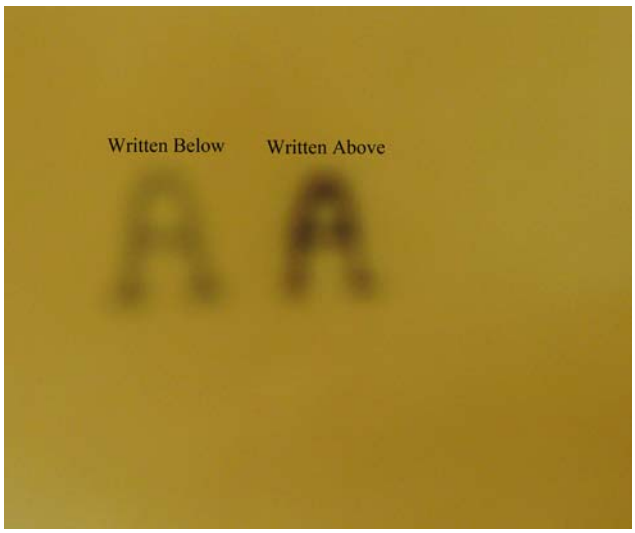


**Fig. 4** A photograph showing the retention of transparency

matrix by the organo MMT layers which increases the tensile strength [4]. The hydrogen bonding as well as chemical linkages (Scheme 1) between clay layers and HBPU matrix at the interface is responsible for this improvement [24]. In HBPU5, the highest tensile strength of 48 MPa was obtained which may be due to high loading along with exfoliated structure formation as supported by the XRD and TEM results. The formation of exfoliated nanoclay structure enhances the interface interactions through bridge, loop, and tail linkages of the polymer chains with the nanoclay layers via H bonding and polar–polar interactions (Scheme 1). Thus, the optimum strength was obtained for HBPU5. Again, generally, the tensile strength of polymeric composites increases at an expense of its elongation at break value, and it was observed in these nanocomposites also. This decrement is due to the restricted movement of the clay layers in the matrixes by the above interactions. However, the decrement is not very high, as the PCL moiety assists the deformation to a certain extent by its flexible chain [25].

Another achievement observed in these nanocomposites is the retention of the flexibility (Table 1). The films can be easily bent to 5 mm parallel mandrel without any damage. The long fatty acid chain of the *Mesua ferrea* L. seed oil and PCL moiety are contributed to this flexibility. Mechanical properties like impact and scratch hardness are seen to be increased notably for all the nanocomposites films compared with the HBPU. This may be due to the overall enhancement of the tensile strength of these flexible films.

The adhesive strength of the nanocomposites was investigated on wood substrate (Table 1). An increase in the strength with the loading of the clay was observed. This may be due to the presence of large numbers of end functionality of the hyperbranched polymer along with other polar groups in the systems. The increment of adhesive strength may be due to the strong interactions of polar hydroxyl, epoxy, urethane, ether, and other polar groups of the epoxy-cured HBPU/clay system with the hydroxyl groups of the substrate [26].

## Water Vapor Barrier Property

Many useful properties of the polyurethane systems are greatly influenced by water absorption phenomena by polyurethane films. Thus, it is essential to study the water vapor loss of the closed system through the films. The barrier property of the clay nanocomposites films is enhancing due to the tortuous diffusion pathway offered by the matrix in the presence of nanoclay layers [27]. The Fig. 5 shows that the water vapor loss decreases significantly with incorporation of clay compared with the HBPU films. Along with the increase in the path of penetration, the MMT layers also increases the cross-linking density thereby reducing the free volume in the cured HBPU matrix. Further, the MMT also improves the phase morphology of the nanocomposites by forming a network structure, which in turn decreases the water absorption property [11].

## Thermal Analysis

The thermal properties of the nanocomposites were studied by DSC and TGA. The glass transition temperature ($T_g$), melting temperature ($T_m$), and melting enthalpy ($\Delta H_m$) were shown in the Table 2. However, in the case of $T_g$ value, the distinct hump formation was not observed in the DSC curve and was taken after zooming the curve. Thus, these $T_g$ values may not be 100% correct, rather presented a rough idea about the flexibility of the soft segment. It was observed that the $T_g$ value increases from −41 °C (for pristine polymer) to −32 °C on adding the nanoclay. The restriction on the segmental chain movement imposed by

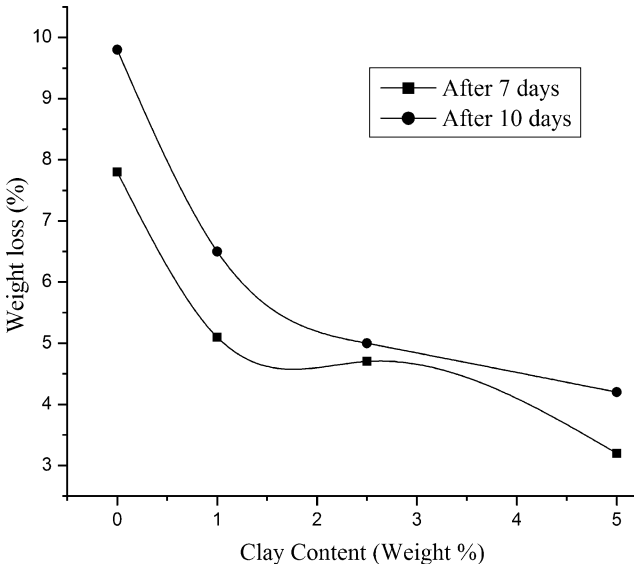


**Fig. 5** Water vapor permeability of the nanocomposites and HBPU

clay particles is the cause for this behavior [1]. A slight increment of melting temperatures from 53 to 56 °C with increase in the clay content of the nanocomposites is observed compared with the pristine polymer (50 °C). This may be due to the formation of compact structure that is formed through different types of molecular interactions as stated earlier with loading of the nanoclay. A miniature increase of the $\Delta H_m$ value with increase in the clay content is noticed, which may result from the small enhancement in the degree of crystallinity of the PCL moiety where the exfoliated nanoclay is acting as a nucleating agent [28]. This result is in conformity with the observed XRD data.

The relative thermal stability of the nanocomposites is examined by TGA. Two-step degradation pattern (Fig. 6) with an enhanced thermal stability of the nanocomposites compared to pristine polymer is observed. The characteristic thermal degradation temperatures are reported in the Table 3. Temperature shifts of 103, 35, and 14 °C, respectively, were observed for the first initial decomposition temperature, temperature corresponding maximum rate of weight loss for the first step, and second initial decomposition temperature with respect to the pristine polymer. This is due to the restricted motion of the polymer chain and the longer path of diffusion for volatiles offered by the clay layers [29]. It is also noticeable that not only the initial decomposition temperature increases but also the weight residue increases (at 650 °C) with the increase in the clay content (7–12%).

### Shape Memory

The nanocomposites with different loading show excellent shape recovery of 96–99%, out of which 90–95% is attained within about 2 min. The values of the shape memory properties of clay nanocomposites were given in Table 2. The increased stored energy due to the incorporation and uniform distribution of clay layers in the HBPU matrix may attribute to this excellent shape memory property [30]. The shape recovery increases with the increase in the clay content which is due to an increase in stored elastic strain energy by clay layers; therefore, while reheating the samples, the film can obtain higher recovery stress due to the release of stored elastic strain [31].

### Chemical Resistance Test

Various chemical environments such as aqueous 10% NaCl, 20% EtOH, 5% HCl, 2% NaOH solutions, and fresh water were used to investigate the effect of these chemical media on the nanocomposites films. The coated glass plates were kept in a 100-mL amber bottle containing the aforesaid media at ambient temperature, (25 ± 2) °C. An excellent chemical resistance was shown by all the nanocomposites for different media (Table 4). This may be due to compact structure, longer diffusion path, and cross-linked structure of the systems.

## Conclusions

The study shows in situ preparation of nanocomposites from *Mesua ferrea* L. seed oil-based hyperbranched polyurethane and nanoclay offers partially exfoliated structure. The formation of nanocomposites significantly improved the performance characteristics like mechanical properties, thermostability, adhesive strength, shape memory behavior, chemical resistance, etc., without much affecting the impact

**Table 2** Thermal properties and shape memory of nanocomposites and pristine polymer

| Sample codes | Glass transition temperature ($T_g$ °C) | Melting temperature ($T_m$ °C) | Melting enthalpy ($\Delta H_m$ J/g) | Shape retention (%) | Shape recovery (%) |
|---|---|---|---|---|---|
| HBPU | −41 | 50 | 58.3 | 84.20 | 97 |
| HBPU1 | −32 | 53 | 55.8 | 83.8 | 98.3 |
| HBPU2.5 | −34 | 54 | 54.4 | 82.5 | 98.9 |
| HBPU5 | −35 | 56 | 53.7 | 82.0 | 99.1 |

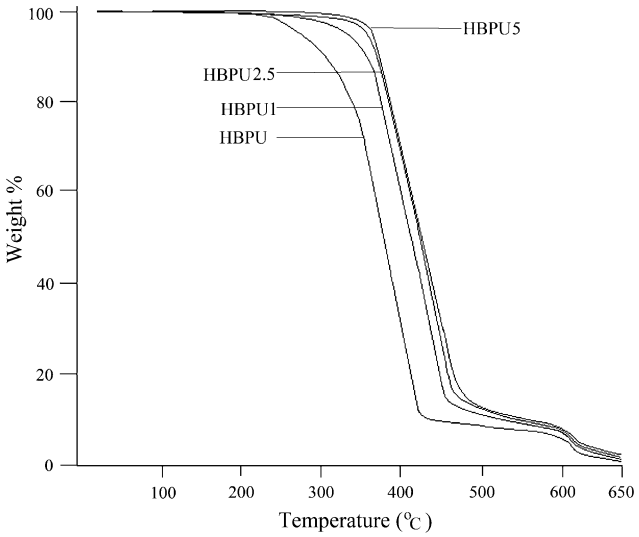


**Fig. 6** Thermogravimetric curves of the nanocomposites and HBPU

**Table 3** Thermal stability data of the nanocomposites and pristine polymer

| Sample code | $T_{1ON}$ | $T_{1MAX}$ | $T_{1END}$ | $T_{2ON}$ | $T_{2MAX}$ | $T_{2END}$ |
|---|---|---|---|---|---|---|
| HBPU | 243 | 350 | 451 | 586 | 597 | 610 |
| HBPU1 | 346 | 385 | 463 | 600 | 611 | 618 |
| HBPU2.5 | 349 | 404 | 465 | 610 | 621 | 629 |
| HBPU5 | 354 | 412 | 469 | 613 | 625 | 631 |

**Table 4** Chemical resistance of the nanocomposites and pristine polymer

| Sample code | 10% NaCl | 20% EtOH | 5% HCl | 2% NaOH | Water |
|---|---|---|---|---|---|
| HBPU | −0.022 | −0.013 | 0.008 | −0.035 | 0.016 |
| HBPU1 | −0.012 | −0.005 | 0.004 | −0.021 | 0.009 |
| HBPU2.5 | −0.007 | −0.003 | 0.002 | −0.023 | 0.011 |
| HBPU5 | −0.004 | −0.002 | 0.006 | −0.022 | 0.014 |

resistance and ductility. Thus study indicates the potentiality of these materials as advanced materials in various fields.

**Acknowledgment** The authors express their gratitude to the research project assistance given by DST, India through the grant No. SR/S3/ME/13/2005-SERC-Engg, dated 9th April, 2007.

## References

1. S.S. Ray, M. Okamoto, Prog. Polym. Sci. **28**, 1539 (2003). doi:10.1016/j.progpolymsci.2003.08.002
2. A. Usuki, N. Hasegawa, M. Kato, Adv. Polym. Sci. **179**, 135 (2005)
3. N. Karak, J. Polym. Mater. **23**, 1 (2006)
4. A. Ganguly, A.K. Bhowmick, Nanoscale Res. Lett. **3**, 36 (2008). doi:10.1007/s11671-007-9111-3
5. R. Xu, E. Manias, A.J. Snyder, J. Runt, Macromolecules **34**, 337 (2001). doi:10.1021/ma0013657
6. T.-K. Chen, Y.-I. Tien, K.-H. Wei, Polymer (Guildf) **41**, 1345 (2000). doi:10.1016/S0032-3861(99)00280-3
7. Y.I. Tien, K.H. Wei, Macromolecules **34**, 9045 (2001). doi:10.1021/ma010551p
8. Q. Sun, F.J. Schork, Y. Deng, Compos. Sci. Technol. **67**, 1823 (2007). doi:10.1016/j.compscitech.2006.10.022
9. C.B. Wang, S.L. Cooper, Macromolecules **16**, 775 (1983). doi:10.1021/ma00239a014
10. J.T. Garrett, J. Runt, J.S. Lin, Macromolecules **33**, 6353 (2000). doi:10.1021/ma000600i
11. Q.M. Jia, M. Zheng, H.X. Chen, R.J. Shen, Polym. Bull. **54**, 65 (2005). doi:10.1007/s00289-005-0372-7
12. M. Song, H.S. Xia, K.J. Yao, D.J. Hourston, Eur. Polym. J. **41**, 259 (2005). doi:10.1016/j.eurpolymj.2004.09.012
13. N. Karak, S. Maiti, *Dendrimers and Hyperbranched Polymers—Synthesis to Applications* (MD Publication Pvt. Ltd., New Delhi, 2008)
14. L. Hong, Y. Cui, X. Wang, X. Tang, J. Appl. Polym. Sci. Part A Polym. Chem. **40**, 344 (2002). doi:10.1002/pola.10102
15. A. Kumar, S. Ramakrishnan, J Chem Soc Chem Commun 453 (1993)
16. S. Unal, I. Yilgor, E. Yilgor, J.P. Sheth, G.L. Wilkes, T.E. Long, Macromolecules **37**, 7081 (2004). doi:10.1021/ma049472e
17. N. Karak, S. Rana, J.W. Cho, J. Appl. Polym. Sci. **112**, 736 (2009). doi:10.1002/app.29468
18. N. Dutta, N. Karak, S.K. Dolui, Prog. Org. Coat. **49**, 146 (2004). doi:10.1016/j.porgcoat.2003.09.005
19. S. Dutta, N. Karak, Polym. Int. **55**, 49 (2006). doi:10.1002/pi.1914
20. S. Dutta, N. Karak, Prog. Org. Coat. **53**, 147 (2005). doi:10.1016/j.porgcoat.2005.02.003
21. A. Ganguly, A.K. Bhowmick, J. Mater. Sci. **44**, 903 (2009). doi:10.1007/s10853-008-3183-z
22. X. Dai, J. Xu, X. Guo, Y. Lu, D. Shen, N. Zhao, X. Luo, X. Zhang, Macromolecules **37**, 5615 (2004). doi:10.1021/ma049900g
23. N.G. Sahoo, Y.C. Jung, H.J. Yoo, J.W. Cho, Macromol. Chem. Phys. **207**, 1773 (2006). doi:10.1002/macp.200600266
24. W.J. Choi, S.H. Kim, Y.J. Kim, S.C. Kim, Polymer (Guildf) **45**, 6045 (2004). doi:10.1016/j.polymer.2004.06.033
25. B. Lepoittevin, M. Devalckenaere, N. Pantoustier, M. Alexandre, D. Kubies, C. Calberg, R. Jerome, P. Dubois, Polymer (Guildf) **43**, 4017 (2002). doi:10.1016/S0032-3861(02)00229-X
26. M.M. Rahman, H.J. Yoo, C.J. Mi, H.D. Kim, Macromol. Symp. **251**, 249 (2007)
27. M.A. Osman, V. Mittal, M. Morbidelli, U.W. Suter, Macromolecules **36**, 9851 (2003). doi:10.1021/ma035077x
28. B. Chen, J.R.G. Evans, Macromolecules **39**, 747 (2006). doi:10.1021/ma052154a
29. S. Kumari, A.K. Mishra, A.V.R. Krishna, K.V.S.N. Raju, Prog. Org. Coat. **60**, 54 (2007). doi:10.1016/j.porgcoat.2007.07.001
30. S. Rana, N. Karak, J.W. Cho, Y.H. Kim, Nanotechnology **19**, 495707 (2008). doi:10.1088/0957-4484/19/49/495707
31. Q.Q. Ni, C.S. Zhang, Y. Fu, G. Dai, T. Kimura, Compos. Struct. **81**, 176 (2007). doi:10.1016/j.compstruct.2006.08.017